A Distributed Automatic Control Framework for Simultaneous Control of Torque and Cadence in Functional Electrical Stimulation Cycling

Ehsan Jafari and Abbas Erfanian

***Abstract*— One of the major challenges facing functional electrical stimulation (FES) cycling is the design of an automatic control system that addresses the problem of disturbance with unknown bound and time-varying behavior of the muscular system. The previous methods for FES-cycling are based on the system modeling and require pre-adjustment of the control parameters which are based on the model parameters. These will degrade the FES-cycling performance and limit the clinical application of the methods. In this paper, a distributed cooperative control framework, which is based on an adaptive higher-order sliding mode (AHOSM) controller, is proposed for simultaneous control of torque and cadence in FES-cycling. The proposed control system is free-model which does not require any pre-adjustment of the control parameters and does not need the boundary of the disturbance to be known. Another major issue in FES-cycling is the stimulation pattern. In the paper, an automatic pattern generator is proposed which is capable of providing not only the regions of the crank angle in which each muscle group should be stimulated but also a specific gain for each muscle group. The results of the simulation studies and experiments on three spinal cord injuries showed that the proposed control strategy significantly increases the efficiency and tracking accuracy of motor-assisted FES-cycling in paraplegic patients and decreases the power consumption compared to HOSM controller with the fixed stimulation pattern. Reducing power consumption can slow down muscle fatigue and consequently increase cycling endurance. The average of cadence and torque tracking errors over three subjects using the proposed method are 5.77±0.5% and 5.23±0.8%, respectively.**

***Index Terms*— Adaptive control, FES-cycling, functional electrical stimulation (FES), fuzzy logic control (FLC), higher order sliding mode (HOSM).**

I. Introduction

FUNCTIONAL electrical stimulation (FES) with a history of more than 50 years, is one of the most commonly used techniques for therapy, restoration and maintenance of vital functions in persons with upper motor neuron disease and intact lower motor neurons [1]. By applying low-level electrical pulses to paralyzed muscles and generating artificial contractions, FES can restore movements like standing, walking, and cycling in lower limbs of spinal cord injury (SCI) patients. Cycling has two main advantages over standing and walking which are safety and generality. FES-cycling is performed in a recumbent position, so the danger of sudden falls and subsequent physical injuries such as bone fractures and traumatic brain injury is less than other types of exercise. Moreover, FES-cycling can be performed at first stages of rehabilitation and even by patients with higher level of paralysis such as tetraplegics [2].

FES-cycling exercise has provided various physiological and psychological benefits for SCI patients. Improvements were reported in cardiovascular and pulmonary functions, peripheral circulation, muscle bulk and strength, gas exchange kinetics and aerobic metabolism, immune system function, and patients' satisfaction and independency in daily life activities [3]–[8].

In spite of the therapeutic and medical benefits of FES-cycling exercise, this technique suffers from several issues. One critical issue in FES-cycling is the stimulation pattern of the muscle groups, i.e., the ranges of crank angle where each muscle group is stimulated. Trial and error is the most common technique for determining the stimulation pattern [2], [9]–[11]. In this technique, the stimulation patterns are obtained for each muscle group at various fixed crank angles by manual determination of the crank angles where maximum positive torque is generated by stimulation of that muscle group. Meanwhile, the accuracy of this technique is entirely dependent on the knowledge of the clinical expert and adjustment of the stimulation pattern at the beginning of each session is exhausting for both patient and medical staff.

Alternative approaches to determine the stimulation pattern are based on model simulation and optimizing a cost function [12]–[16]. In [13], based on a dynamic model of planar recumbent pedaling, the ON and OFF times of the electrical stimulation and the stimulation amplitude were computed such that the muscle fatigue was minimized.

Minimizing the muscle fatigue [14], maximizing the average active power generated at the crank with lowest muscle force [15], and minimizing the ratio of the metabolic energy consumption to the mechanical power generated at the crank during cycling [16], were also considered for determining the ON and OFF times of the stimulation signal.

Manuscript received 10 October 2021; revised 8 March 2022, 23 April 2022, and 3 June 2022; accepted 28 June 2022. Date of publication 6 July 2022; date of current version 15 July 2022. *(Corresponding author: Abbas Erfanian.)*

This work involved human subjects or animals in its research. Approval of all ethical and experimental procedures and protocols was granted by the Ethics Committee of Iran Neural Technology Research Center.

Ehsan Jafari is with the Iran Neural Technology Research Center, Department of Biomedical Engineering, Iran University of Science and Technology, Tehran 1684613114, Iran (e-mail: e_jafari47@yahoo.com).

Abbas Erfanian is with the Iran Neural Technology Research Center, Department of Biomedical Engineering, School of Electrical Engineering, Iran University of Science and Technology, Tehran 1684613114, Iran (e-mail: erfanian@iust.ac.ir).

Digital Object Identifier 10.1109/TNSRE.2022.3188735

In [20], the system's Jacobian elements (i.e., muscle group torque transfer ratio) was used to determine the ON and OFF times for stimulation of the gluteal, quadriceps femoris, and hamstrings muscles. In this method, the length of leg segments (thigh and shank) of each patient and geometric properties of the recumbent stationary cycle (the vertical and horizontal seat position, and length of crank) were measured to determine each muscle group transfer ratio. The stimulation for each muscle group was ON only when the corresponding Jacobian element was greater than a threshold value which was determined by a trial-and-error method.

Another challenge facing the control of FES-cycling is the time-varying and non-linear properties of the electrically stimulated muscle. These properties limit the utility of the open-loop approach for control of FES. To cope with these problems, several closed-loop control strategies for FES-cycling have been proposed by the researchers [9], [14], [17], [20]–[30].

Chen *et al.* [17] examined a fuzzy logic control with fixed-parameter feedback control method to control the FES-cycling cadence. Hunt *at al.* [9] proposed a closed-loop control which was based on the pole assignment procedure, for control of both cycling cadence and leg power output. However, it should be noted that the performance of the pole placement approach requires an accurate linear model of the system. Kim *et al.* [14] proposed a control strategy in which a quasi-joint torque was first computed using an inverse model of musculoskeletal system and a proportional and derivative (PD) control and then the optimal muscle force for each muscle was estimated using a static optimization method to minimize the muscle fatigue. The optimal values of the PD control was determined by the genetic algorithm. The proposed method has not yet been investigated on human subjects.

Bellman *et al.* proposed a switching control strategy based on the first-order sliding mode control (SMC) for controlling the cycling cadence [20], [21] and simultaneous cadence and power tracking [22]. SMC is a nonlinear control scheme which is inherently robust against the time-varying behavior of the system with bounded and known disturbances [18], [19]. However, the drawback of the first order SMC is the chattering which is caused by the high frequency oscillations in the control input [23]. Moreover, conventional SMC can only guarantee the asymptotic stability; hence, the error cannot converge to zero in finite time. Furthermore, implementation of the first-order SMC requires canonical presentation of the plant to be controlled. Identification of such model is a critical issue facing the first-order SMC.

Repetitive learning control (RLC) with a robust feedback term [24]–[26] as well as iterative learning control (ILC) with a robust feedback term [27] has been proposed for control of FES-cycling to track a desired cadence [24], [25], [27] or to track a desired torque trajectory [26]. However, RLC and ILC cannot provide perfect tracking in every situation [28], [29]. More important, unstructured uncertainties and nonrepeating disturbances hinder the control performances. Moreover, RLC requires an internal model of the reference/disturbance to enable rejection of a repeating disturbance as well as asymptotic convergence to a desired reference trajectory [30]. In addition, the methods proposed in [24]–[27] provide asymptotic convergence. To ensure the system stability, the control parameters should be set based on the parameters of the cycle-rider dynamic model that should be known. Furthermore, the bound of disturbance should be known.

To tackle the aforementioned problems, higher-order sliding mode (HOSM) technique has been already proposed for control of FES-cycling in SCI patients [31] and control of a hybrid FES/electric motor knee extension system [44], [45]. The HOSM approach has been proposed for reducing chattering implemented with continuous control action while robustness is preserved [32], [33].

The main challenge of the *rth-order sliding mode* controller is that it requires the knowledge of the sliding variable derivatives up to the $(r-1)$ th order. However, the super-twisting control (STW) which is a second-order continuous sliding mode control, does not need the time derivative of the sliding variable [19], [33]. The STW algorithm provides a continuous control action that derives both the sliding variable and its derivative to zero in finite time even in the presence of the disturbances [32], [33]. However, the STW algorithm requires the boundary of the disturbance gradient to be known. But, in many practical cases, it is difficult to estimate this boundary. This leads to set a large value to the control gain of the controller to ensure the finite-time convergence. The overestimating of the controller gain will cause to increase the chattering [34]. In previous work [31], we applied the super-twisting (STW) algorithm for controlling the FES-pedaling.

The first aim of this paper is to cope with the aforementioned problem related to STW control law. For this purpose, we adopt an adaptive-gain STW (ASTW) algorithm that is able to generate continuous control action and its gains are adaptively tuned in real-time with respect to the disturbance with unknown boundary. The second objective is to propose a new automatic Jacobian-based stimulation pattern generator which is only based on joint angles and crank angle and does not require anthropometric characteristics of patients or optimization of any cost function.

II. Methods

Fig.1 shows the structure of the proposed distributed control framework. Three autonomous controllers distributed through the system for simultaneous control of both cycling cadence and leg torque. One HOSM was designed for regulating DC-motor input to control the cadence and an adaptive HOSM for adjusting the pulse-width of the muscle stimulation for control of the leg torque. Moreover, a fuzzy logic controller (FLC) was designed for regulating the pulse-amplitude. The crank angle was used to activate/deactivate each muscle during each cycle according to the stimulation pattern determined by the proposed method.

A. Adaptive Super-Twisting Sliding Mode Controller

Consider a smooth dynamical system described by

$$x^n = f(x,t) + b(x,t)\cdot u \tag{1}$$

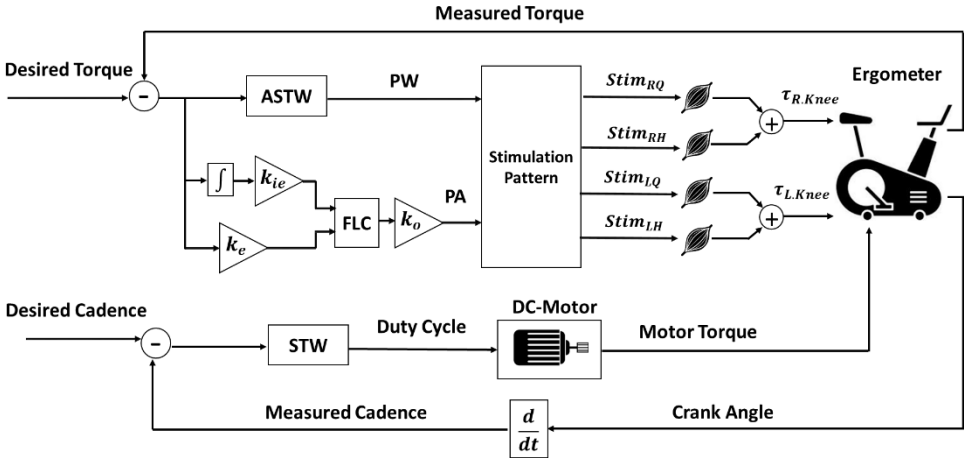

Fig. 1. Block diagram of the proposed stimulation pattern method and control strategy for FES-cycling. k_e, k_{ie}, and k_o are scaling factors of the fuzzy logic controller.

where $x \in \Re^n$ is the system state, $u \in \Re$ is the control input, and f and b are unknown smooth nonlinear functions. The first task to design the SMC is to define a sliding variable as follows

$$s(x,t) = \left(\frac{d}{dt} + c\right)^{n-1} e(t) \tag{2}$$

where c is a positive constant and $e(t)$ is the tracking error. If the successive total time derivatives $s = \dot{s} = \ddot{s} = \cdots = s^{(r-1)}$ are continuous functions of the state variable x and the set $s = \dot{s} = \ddot{s} = \cdots = s^{(r-1)} = 0$ is non-empty, then, the motion in manifold $s = \dot{s} = \ddot{s} = \cdots = s^{(r-1)} = 0$ is called the r-sliding mode [19], [35]. It has been shown that implementing the HOSM based on the homogeneity approach yields finite-time convergence and provides highest asymptotic accuracy in the presence of measurement noises, discrete measurement, and switching delays [19], [36]. However, the higher-order sliding mode controller requires high order time derivatives of the sliding variable. To preserve the main advantages of the higher-order sliding-mode approach, the second-order SMC (2-SMC) with super-twisting algorithm is used in this study [33]. This algorithm could reduce the chattering phenomena and to steer s and $\dot{s}$ to zero in finite time by defining a proper control $u(t)$. The control input consists of two continuous terms as follows

$$\begin{aligned} u &= -\lambda |s|^{\rho} sign(s) + u_1 \\ \dot{u}_1 &= -W sign(s) \end{aligned} \tag{3}$$

where u is the control input. It can be pulse width (PW) of the stimulation signal or motor input when the HOSM control is used for control of the leg torque or cadence control, respectively. It is seen that the control input does not require the time derivative of the sliding variable. The convergence of the sliding variable to the sliding surface in finite-time requires the following conditions [33]

$$W > \frac{C_0}{K_m}, \lambda^2 \geq \frac{4C_0}{K_m^2} \frac{K_M (W + C_0)}{K_m (W - C_0)}, 0 < \rho \leq 0.5 \tag{4}$$

where K_m, K_M, and C_0 are positive constants. In this work, the ρ was set to 0.5. The choice $\rho = 0.5$ ensures that the maximal possible for realization of the 2-sliding mode is achieved [33]. The selections of the parameters λ and W need to know the system parameters. But, it is not easy to determine the system parameters. Therefore, a large value should be assigned to the parameters λ and W to achieve robustness and finite time convergence. However, the large value of these parameters will cause chattering and consequently deteriorate the system performance.

Another drawback of the STW algorithm is that it requires the boundary of the disturbance to be known. In many practical cases, this boundary cannot be easily estimated. Therefore, the control gain must be set a large value to guarantee finite-time convergence. To overcome this problem, adaptive-gain STW (ASTW) algorithm has been proposed such that its gains are adaptively tuned in real-time. The main advantage of ASTW is the finite-time convergence in the presence of the bounded additive and multiplicative perturbations with unknown boundaries [34]. In ASTW algorithm, the gains are adapted according to the following adaptation law

$$\begin{aligned} \lambda &= \lambda(s, \dot{s}, t) \\ W &= W(s, \dot{s}, t) \\ \dot{\lambda} &= \begin{cases} \omega \sqrt{\frac{\gamma}{2}} sign(|s| - \phi), & \text{if } \lambda > \lambda_m \\ \eta, & \text{if } \lambda \leq \lambda_m \end{cases} \end{aligned} \tag{5}$$

$$W = \varepsilon \cdot \lambda \tag{6}$$

where ε, γ, ω, η are arbitrary positive constants. The right side of (6) and ε can be considered as the learning rates of the adapting parameters λ and W. In ASTW, the control gains $\lambda(t)$ and $W(t)$ dynamically increase until the sliding variable and its derivative reach the sliding surface and then begin to decrease. The gains will begin to increase when the sliding variable or its derivative start deviating from the equilibrium point $s = \dot{s} = 0$. This idea was designed in ASTW by introducing a domain $|s| \leq \varphi$ in (6). As soon as the sliding variables reach this domain, the control gains start to decrease until the sliding variables leave the domain. The parameter λ_m is an arbitrary small positive constant (details can be found in [34]).

TABLE I
MEMBERSHIP FUNCTIONS PARAMETERS FOR THE FUZZY LOGIC CONTROLLER

	σ	c_1	c_2	c_3	c_4	c_5
$e, \int e$	0.25	-1	-0.5	0	0.5	1
I	0.05	0.50	0.625	0.75	0.875	1

TABLE II
FUZZY RULES FOR FUZZY ADJUSTMENT OF THE PULSE AMPLITUDE

e \ $\int e$	NB	N	Z	P	PB
NB	SB	SB	SB	S	M
N	SB	SB	S	M	L
Z	SB	S	M	L	LB
P	S	M	L	LB	LB
PB	M	L	LB	LB	LB

N: Negative, P: Positive; S: Small; M: Medium; L: Large; Z: Zero, PB: Positive big; SB: Small big; NB: Negative big.

B. Fuzzy Logic Control

In the current study, a FLC is used to regulate the pulse amplitude (PA) of the stimulation signal [37]. The error signal (e) and the integral of the error ($\int e$) are used as the inputs of the FLC and the PA as the output.

Fuzzy membership functions are selected as follows

$$\mu_A^j(x_i) = \exp\left[-\left(\frac{x_i - c^j}{\sigma^j}\right)^2\right] \tag{7}$$

where "A" is one of the fuzzy sets. c^j and σ^j are the mean and the standard deviation of the jth Gaussian membership function, respectively, and x_i represents e or $\int e$. The membership functions parameters (i.e., c^j, σ^j) are fixed and tabulated in Table I. The membership functions are uniformly distributed with 50% overlap over the domain of the variables. In this work, the maximum current level has been set to 110 mA. This was selected to be tolerable for all subjects. Therefore, according to the member function parameters (Table I), PA could vary from 55 to 110 mA.

The inference engine maps the input fuzzy sets to an output fuzzy set using the pre-defined rules (Table II). Finally, the final output of the FLC (i.e., defuzzification step) is computed as follows:

$$y = \frac{\sum_{j=1}^{r} \mu_A^j \cdot y_j}{\sum_{j=1}^{r} \mu_A^j} \tag{8}$$

where μ_A^j is the membership value of the jth rule, y_j is the output of the jth rule, and r is the number of the total fuzzy rules. The performance of the FLC can be tuned through three scaling parameters k_e, k_{ie}, and k_o (Fig. 1).

C. Stimulation Pattern

In this section, a simple and easy algorithm based on the joint angles is proposed to determine the ON and OFF stimulation times. The contribution of each joint torque to the crank torque can be expressed as follows [38]:

$$\tau_{cr} = \frac{\partial \theta_h(q)}{\partial q}\tau_h + \frac{\partial \theta_k(q)}{\partial q}\tau_k, \quad \forall q \in [0, 2\pi] \tag{9}$$

where q is the crank angle, θ_h is the hip angle, θ_k is the knee angle, $\partial\theta_h(q)/\partial q$ is the hip joint torque transfer function, $\partial\theta_k(q)/\partial q$ is the knee joint torque transfer function (i.e., Jacobian element), τ_h, τ_k, and τ_{cr} are the hip, knee, and crank torques, respectively. For forward cycling, each muscle group should be stimulated in a specific range of crank angle to produce forward torque about the crank (i.e., $\tau_{cr} \geq 0$). Each joint is consisted of the flexor and extensor muscle groups and it is not sensible to stimulate them simultaneously because they would counteract themselves and accelerate the fatigue, so in each angle only one of them can be ON and the other should be OFF. Our purpose is to find regions and gains according to the crank angle in which each muscle group should be stimulated to yield positive torque about crank.

In each cycle, there are two specific points for each joint, in which joint angle reaches its maximum and minimum values (i.e., d_{1k} and d_{2k} for the knee joint; d_{1h} and d_{2h} for the hip joint in Fig. 2). As illustrated in Fig. 2(a), to move from d_{1k} (d_{1h}) to d_{2k} (d_{2h}), knee (hip) angle begins to increase from minimum value to maximum value (i.e., knee (hip) extension). Hence, changes of the knee (hip) angle are positive in this region. In contrast, to move from d_{2k} (d_{2h}) to d_{1k} (d_{1h}), knee (hip) angle begins to decrease from maximum value to minimum value (i.e., knee (hip) flexion) and changes of the knee (hip) angle are negative.

In the range of the crank angle from d_{1k} to d_{2k}, $\partial\theta_k(q)/\partial q > 0$. Since $(\partial\theta_k(q)/\partial q)\tau_k > 0$, it follows that $\tau_k > 0$, $\tau_k = \tau_{k.Ext.}$, $\forall q \in [d_{1k}, d_{2k}]$.

In the range of the crank angle from d_{2k} to d_{1k}, $\partial\theta_k(q)/\partial q < 0$. Since $(\partial\theta_k(q)/\partial q)\tau_k > 0$, it follows that $\tau_k < 0$, $\tau_k = \tau_{k.Flex}$, $\forall q \in [d_{2k}, d_{1k}]$, where $\tau_{k.Ext.}$ and $\tau_{k.Flex.}$ are the resultant torques of knee extensor and knee flexor muscle groups, respectively.

In the range of the crank angle from d_{1h} to d_{2h}, $\partial\theta_h(q)/\partial q > 0$. Since $(\partial\theta_h(q)/\partial q)\tau_h > 0$, it follows that $\tau_h > 0$, $\tau_h = \tau_{h.Ext.}$, $\forall q \in [d_{1h}, d_{2h}]$.

In the range of the crank angle from d_{2h} to d_{1h}, $\partial\theta_h(q)/\partial q < 0$. Since $(\partial\theta_h(q)/\partial q)\tau_h > 0$, it follows that $\tau_h < 0$, $\tau_h = \tau_{h.Flex}$, $\forall q \in [d_{2h}, d_{1h}]$, where $\tau_{h.Ext.}$ and $\tau_{h.Flex.}$ are the resultant torques of hip extensor and hip flexor muscle groups, respectively. Therefore, d_{1k} (d_{1h}) and d_{2k} (d_{2h}) can be considered as the ON and OFF (switching) times for the knee (hip) extensor and flexor.

In this study, to compensate for the electromechanical delay of muscle (i.e., the time between the application of electrical stimulation and torque response) the stimulation pattern was shifted 150ms forward in time. Moreover, the normalized absolute value of the torque transfer function at each joint angle can be used as the gain factor for each muscle group

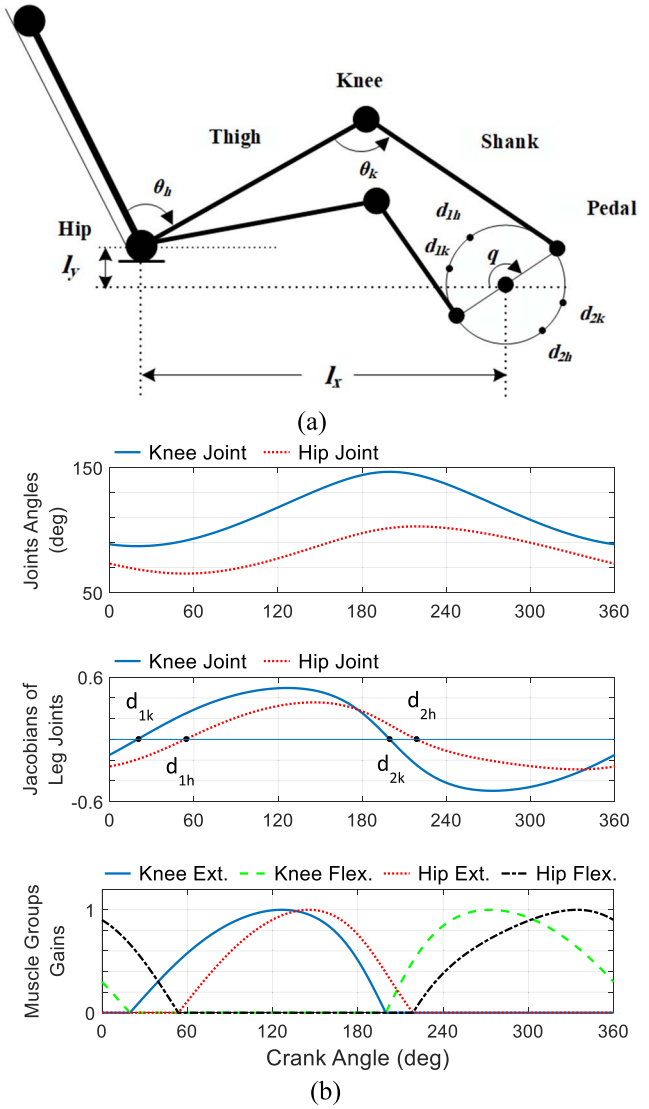

Fig. 2. (a) Skeletal model of the recumbent cycling. θ_h, θ_k, and q are the hip angle, the knee angle, and the crank angle (between crank arm and horizontal line), respectively. l_x and l_y are horizontal and vertical position of the hip joint with respect to the crank center, respectively. (b) d_{1k} (d_{1h}) and d_{2k} (d_{2h}) are the dead points of the right knee (hip) joint which are the switching times of the stimulation between the knee (hip) extensor and the flexor.

(Fig. 2(b)):

$$g_m(q) = \begin{cases} \left|\frac{\partial \theta_j(q)}{\partial q}\right|_{normalized}, & \text{if } q \in [d_i, d_f] \\ 0, & elsewise \end{cases} \quad (10)$$

where m indicates the muscle group, j is the joint, and d_i and d_f define the angles in which a muscle group activated and deactivated, respectively.

D. Motor-Assisted Bicycle-Rider Model

The dynamic model of a two-legged virtual patient pedaling an ergometer can be written as

$$M(q)\ddot{q} + C(q)\dot{q} + G(q) = \sum_{i=r,l} \left[J_{h,i}(q)\tau_{h,i} + J_{k,i}(q)\tau_{k,i}\right] + D + Q \quad (11)$$

where q is the crank angle, $M(q)$, $C(q)$, and $G(q)$ denotes the moment of inertia, the Coriolis and centripetal torque, and the gravitational torque, respectively. $\tau_{h,i}$ and $\tau_{k,i}$ are the active torques generated at the hip and knee joints, respectively. The index i indicates the left or the right leg. These joints torque are transferred to the crank via Jacobian elements $J_h(q)$ and $J_k(q)$. Q is the torque generated by the motor and D represents the effects of the disturbances (i.e., spasticity and friction). The values of the skeletal parameters used in the model are summarized in Table III. In this model, each leg consists of a double pendulum which represents two revolute joints (i.e., hip and knee joints) and two links (i.e., thigh and shank). Hip joint is fixed to the cycle seat and ankle joint is locked by foot orthosis to the pedal for safety and stability. Each foot is attached to one pedal and the two pedals are rotating about the crank with a constant phase difference of 180 degrees. A five-bar closed kinematic chain mechanism can be used to model the bicycle-rider system. The model consists of the right thigh, right shank, crank, left shank, and left thigh. (Fig. 2(a)). According to the fixed end-points (i.e., hip joint, crank center, and cycle frame), for each leg, the closed kinematic chain can be expressed by only one degree of freedom which is crank angle (q) [38], [39].

For each leg, an extensor muscle (quadriceps) and a flexor muscle (hamstrings) were considered. The muscle model proposed in [40] used here to model the two-legged virtual patient. The parameters of the muscle model were taken from [40]. To control the cycling cadence, a model of DC-motor proposed in [41] was employed as follows

$$\frac{d}{dt}\dot{\theta} = -\frac{b}{J}\dot{\theta} + \frac{k_t}{J}i(t) - \frac{1}{J}T_l(t)$$
$$\frac{d}{dt}i(t) = -\frac{r}{l}i(t) - \frac{k_e}{l}\dot{\theta} + \frac{1}{l}v(t) \quad (12)$$

where $\dot{\theta}$ is the shaft angular velocity, $i(t)$ is the phase current, $v(t)$ is the supply voltage, $T_l(t)$ is the load torque, b, l, J, r, k_e, and k_t are the motor parameters. The motor parameters were chosen as follows

$J = 0.01$ kg.m^2, $b = 0.1$ N.m.s/rad, $k_e = 0.01$ V.s/rad, $k_t = 0.01$ N.m/A, $r = 1\Omega$, $l = 0.5$H.

We have used these values in order to be able to compare the results with our previous work [33]. These values were usually used in literature for simulating DC motor as in [46] and [47].

E. Experiments

1) Subjects: Two thoracic-level and one cervical-level complete spinal cord injury subjects participated in this study (Table IV). The patients have been involving in a rehabilitation research program including electrically stimulated exercise of their lower limbs using ParaWalk neuroprosthesis [43]. The FES-cycling experiment session for each subject was performed once a week and each session consisted of at least six 5-min trials with inter-trial resting interval of at least 10 min. All experimental procedures were approved by the Ethics Committee of Iran Neural Technology Research Center and the subjects gave written informed consent.

TABLE III
PARAMETERS OF THE BICYCLE-RIDER MODEL

Weight	$W = 66\ kg$	Height	$H = 1.7\ m$
Length of thigh	$l_t = 0.4165\ m$	Mass of thigh	$m_t = 6.6\ kg$
Length of shank	$l_s = 0.4845\ m$	Mass of shank	$m_s = 3.069\ kg$
Length from hip to thigh COM* (proximal)	$l_{mt} = 0.180\ m$	Thigh moment of inertia w.r.t. COM	$I_t = 0.1194\ kg.m^2$
Length from knee to shank COM (proximal)	$l_{ms} = 0.209\ m$	Shank moment of inertia w.r.t. COM	$I_s = 0.0657\ kg.m^2$
Horizontal length from hip to crank	$l_x = 0.67\ (0.73)\ m$	Vertical length from hip to crank	$l_y = 0\ (0.25)\ m$
Length of crank	$l_{cr} = 0.12\ m$		

*COM = Center of Mass

TABLE IV
CLINICAL PROPERTIES OF SPINAL CORD INJURIES

Subject	Sex	Age	Weight (Kg)	Height (cm)	Injury Level	ASIA* Class	Date of Injury
AA	M	28	93	190	T2-T8	A	2011
HD	M	39	97	178	C7	A	2008
EA	M	34	85	167	T7-T8	A	2006

*American Spinal Injury Association Classification

2) Apparatus and System: An indoor cycling ergometer was adopted and modified for FES-cycling. The torque generated about the crank was measured using a rotary torque sensor (TRD605, Futek Advanced Sensor Technology, Inc, USA). The sensor was also equipped with an incremental encoder with resolution of 720 pulse/turn. An infrared sensor was added to the ergometer to provide an absolute position reference of crank angle. A custom-made stimulator was used to stimulate four muscle groups (i.e. the left and right quadriceps and hamstrings) via self-adhesive electrodes (PROTENS, $5cm \times 9cm$, South Korea). In this work, a hybrid stimulation scheme, which is based on combined pulse-width and pulse-amplitude modulation at a constant frequency ($25Hz$) was used to stimulate the quadriceps and hamstrings. The Xsens motion tracker system MTx (Xsens Technologies, Netherlands) was used to measure the joint angles. The recorded joint angles and crank angle were averaged over a number of cycles. Then, the averaged joint angle was fitted with a six-term Fourier series to find the joint angle in terms of crank angle. Online data acquisition, processing, and generating the control pulses were performed using a custom-built LabVIEW program with the sampling period of $40ms$ for control updates. The u_1 and λ in (3) and (6) were computed using the Point-by-Point VIs in LabVIEW during real-time control.

III. RESULTS

Tracking accuracy was measured using, normalized root mean square (NRMS) of error as follows

$$NRMS\,(\%) = \frac{1}{\max\,(x_d\,(n))}\sqrt{\frac{1}{N}\sum_{n=1}^{N}(x\,(n) - x_d\,(n))^2} \times 100$$

where x_d denotes the desired value, x is measured value, and N is the number of samples. We also used power consumption (PC) as a measure of endurance of the muscle groups involved in the FES-cycling. The PC was defined as the average of stimulus charge per phase over each trial of the experiment. The stimulus charge per phase is defined as the product of pulse-width by pulse-amplitude for rectangular current pulses [48], [49] (The units are millicoulombs or microcoulombs per phase). The PC was defined as follows [11]

$$PC\,(\%) = \frac{1}{N}\sum_{i=1}^{N}\left(\frac{PW\,(i)}{PW_{\max}}\right) \times \left(\frac{PA\,(i)}{PA_{\max}}\right) \times 100 \quad (13)$$

The statistical difference between the results (i.e., tracking accuracy and power consumption) obtained by different methods was assessed by the analysis of variance (ANOVA) and a confidence level of 95% ($p < 0.05$) was selected for detecting significant difference.

The control gains, introduced in (6), were chosen during the simulation study as follows: $\gamma = 2$, $\omega = 0.02$, $\varepsilon = 0.1$, $\eta = \lambda_m = 0.1$ and then used for all the subjects who participated in the experiments on different days. The domain range was selected as $\varphi \in [0.5, 0.9]$ and $\varphi \in [0.07, 0.12]$ during the simulation and experimental studies, respectively.

A. Simulation Results

The proposed schemes are used here to control the cycling cadence and leg torque (power) of a virtual patient with 66kg weight, 170cm height, thigh length of 42cm, and lower leg length of 48cm (Table III). The humanoid dimensions used in this work is based on the standard anthropometric human dimensions introduced in [42]. The length and the mass of each segment of the model are summarized in Table III. The simulations were performed under muscle fatigue and external disturbance and with the fixed stimulation patterns proposed in [17] as well as with the stimulation pattern determined by

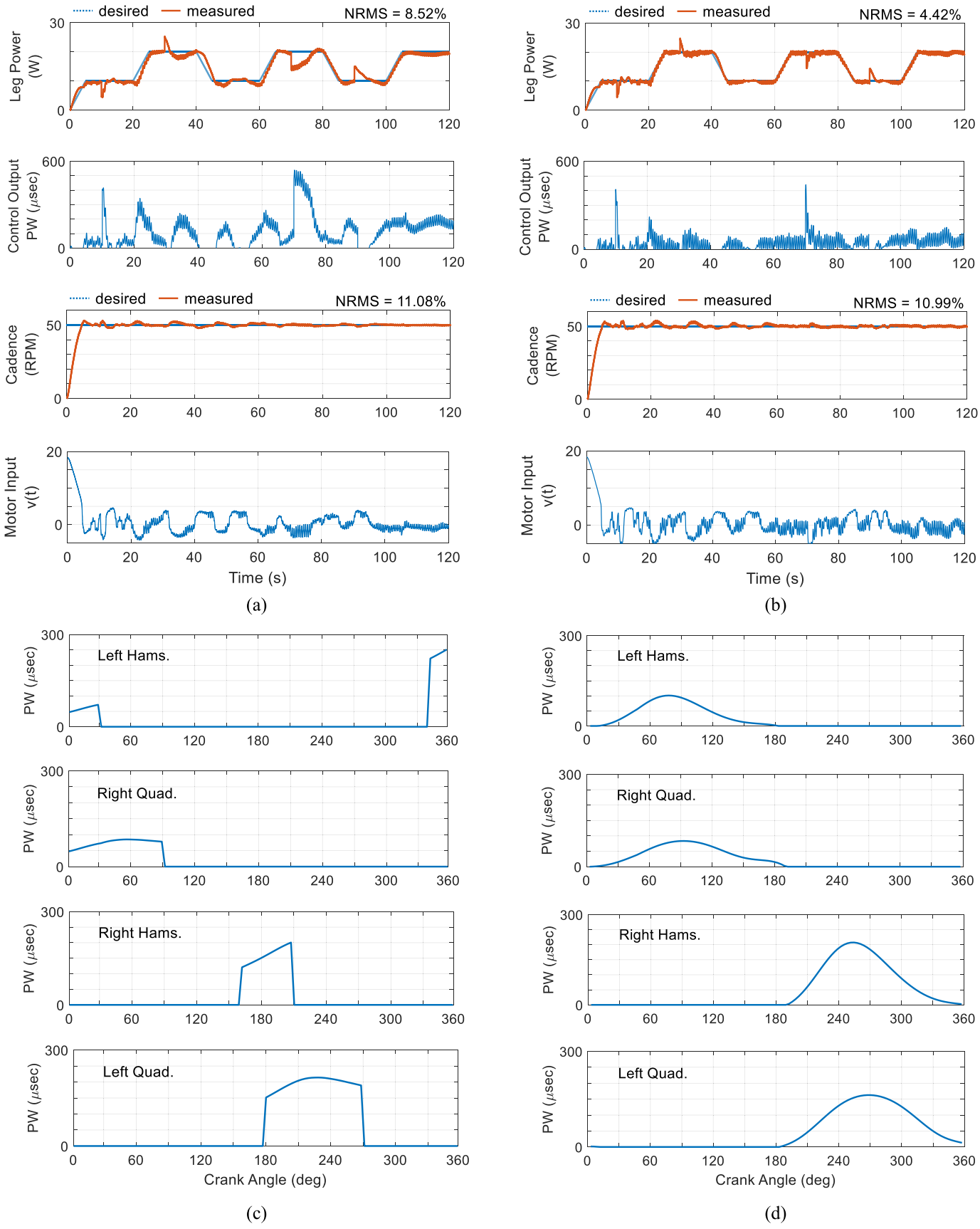

Fig. 3. Simulation results of the leg power and cadence tracking control using ASTW and STW, respectively, with the fixed and the proposed stimulation patterns while the muscle fatigue and the external disturbance were simultaneously applied. (a) Fixed stimulation pattern. (b) Proposed stimulation pattern. (c) Input of the muscle groups when the fixed stimulation pattern was used. (d) Input of the muscle groups when the proposed stimulation pattern was used.

the proposed method in this work. The desired trajectory of the leg power was varied between 10 Watt and 20 Watt in a trapezoidal fashion while the reference signal for the cadence was kept at constant value of 50 PRM which was pervasive in FES-cycling literature [6], [9]. Instantaneous leg power was computed as the product of the crank torque and cadence.

During simulation, the output of the controller (i.e., ASTW) was multiplied by a constant gain as in [40] and the result was considered as the muscle input (i.e., PW). In this study, the constant gain was set to be 250 μsec. The muscle model used in this study had only one variable to control the muscle force [40]. Therefore, only the ASTW controller was used to control the muscle force. For control of cadence, the output of the controller (i.e., STW) was directly applied to the input of the DC-motor (i.e.,$\upsilon(t)$). Fig. 3 shows the results of tracking control using ASTW with the stimulation patterns determined by the proposed method as well as by the fixed stimulation pattern, while both muscle fatigue and the external disturbance were applied. It was reported that in electrically stimulated muscle, fatigue can cause a drop in peak muscle torque, approximately 50% reduction over 100 s [40]. Accordingly, in this paper, the effect of the muscle fatigue was assessed by asymptotic decreasing the muscle's input gain to 75% of its initial value over 120 s.

External disturbance rejection was evaluated by subtracting a constant torque in amount of 1Nm from the torque acting on the crank for a duration of 20 s at 10 s and 70 s, respectively. The tracking errors achieved are 4.42% and 10.99% for the leg power and cycling cadence, respectively, using the proposed stimulation pattern, while they are 8.52% and 11.08% using the fixed stimulation pattern. The results indicate that the power consumption incurred by the proposed stimulation pattern (16.44%) is much lower than that by the fixed stimulation pattern (41.86%). The muscle inputs using the fixed stimulation pattern and the proposed pattern during a complete 360-degree cycle are shown in Fig. 3(c) and (d), respectively. The muscle input is obtained by multiplication of the control output by the stimulation pattern (Figs. 3(a) and (b)). It is clearly observed in Fig. 3(d) that a smooth muscle input is obtained using the proposed stimulation pattern.

Fig. 4(a) and (b) show the proposed stimulation pattern and the pattern proposed in [17] for the virtual patient with the specification summarized in Table III while $l_y = 0$ cm and $l_x = 67$ cm. The stimulation pattern estimated by the proposed method are shown in Fig. 4(c) while $l_y = 25$ cm and $l_x = 73$ cm. The proposed method has determined the ON and OFF times of the stimulation as well as the muscle gain for each muscle. As illustrated in Fig. 4, the proposed method could determine exclusive stimulation patterns under different physical conditions of subject and bicycle.

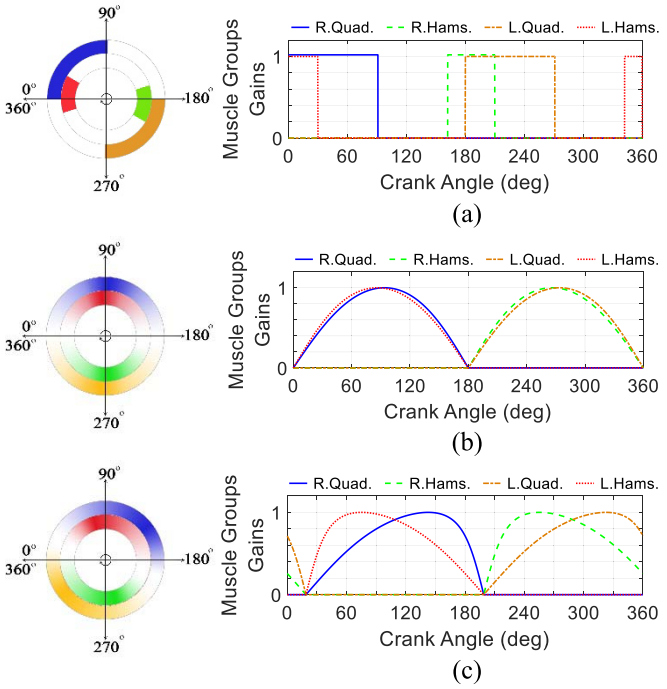

Fig. 4. Stimulation patterns. (a) Fixed stimulation pattern [17]. (b) Proposed stimulation pattern when $l_y = 0$ cm and $l_x = 67$cm. (c) Proposed stimulation pattern when $l_y = 25$ cm and $l_x = 73$ cm.

B. Experimental Results

Fig. 5(a) shows examples of the motor cadence control and leg torque control during a 300-s trial of FES-pedaling using ASTW with the proposed stimulation pattern for the paraplegic subject AA. The results show that a good tracking control for both cycling cadence and leg torque was achieved. The torque and cadence tracking errors during this trial of cycling are 4.00% and 5.11%, respectively. It is observed that cycling cadence converges to the desired value in less than 3 seconds at the start of the experiment. The control action is smooth without having high-frequency oscillations and no chattering is observed in the leg torque and cycling cadence. By passing the time, the controller automatically increases the stimulation intensity (i.e., PW and PA) to compensate for the effect of the muscle fatigue. Muscle fatigue causes reduction in muscle force over time. Therefore, the controller inevitably increases the stimulation intensity to be able to track the desired torque. Note that the stimulation PW and PA are adjusted by the ASTW and FLC, respectively. The same information as in Fig. 5(a) is shown in Fig. 5(c) using STW controller. A weak chattering is appeared in the leg torque and cycling cadence. In this case, the torque and cadence tracking errors during this trial of cycling are 4.82% and 5.53%, respectively. The power consumption incurred by ASTW and STW algorithms are 36.17% and 39.07%, respectively. Fig. 5(b) and (d) shows the tracking results for the same subject using ASTW and STW algorithm using fixed stimulation pattern, respectively. The results show that the tracking error and chattering increase compared to the results obtained by the proposed stimulation pattern. Moreover, the power consumed by the fixed stimulation pattern is much higher than that by the proposed stimulation pattern. In this case, the power consumptions are 48.28% and 53.54% using ASTW and STW algorithms, respectively.

The stimulation patterns obtained by the proposed method and manual adjustment are shown in Fig. 6. It can be seen that the stimulation pattern obtained by the proposed method provides a soft switching between the muscles. Although one

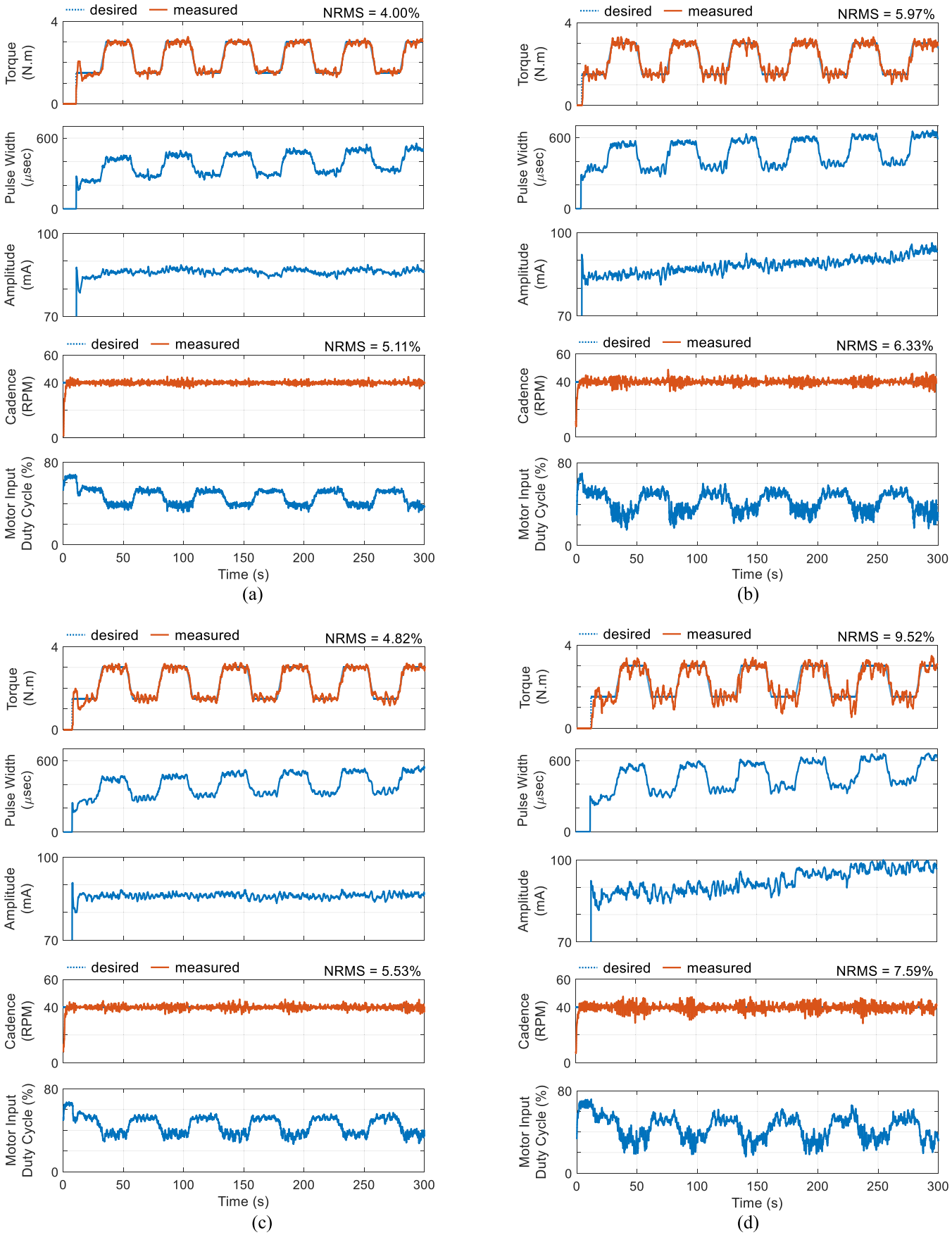

Fig. 5. Leg torque and cadence control using the fixed and the proposed stimulation patterns for subject AA. (a) ASTW with the proposed stimulation pattern. (b) ASTW with the fixed stimulation pattern. (c) STW with the proposed stimulation pattern. (d) STW with the fixed stimulation pattern.

TABLE V

AVERAGE OF THE NORMALIZED RMS TORQUE TRACKING ERROR (%) USING ASTW AND STW CONTROLLERS WITH BOTH THE FIXED AND THE PROPOSED STIMULATION PATTERNS ON THREE SPINAL CORD INJURY SUBJECTS FOR THREE DAYS

Stimulation Pattern	Subject	ASTW				STW			
		Day1	Day2	Day3	mean	Day1	Day2	Day3	mean
Proposed	AA	4.25±0.4	4.35±0.7	4.48±0.7	4.36±0.5	4.93±0.1	5.76±0.1	5.08±1.3	5.25±0.7
	HD	4.96±0.1	5.67±0.2	5.67±0.6	5.43±0.5	5.53±0.4	6.25±0.3	6.04±0.4	5.94±0.4
	EA	5.14±0.6	6.33±0.4	6.15±0.3	5.87±0.7	5.89±0.5	7.55±0.6	6.42±0.6	6.62±0.9
	Average	5.23±0.8				5.94±0.9			
Fixed	AA	7.09±0.2	7.06±0.1	6.12±02	6.75±0.5	9.86±1.4	9.61±0.1	8.82±0.4	9.43±0.8
	HD	8.56±0.1	7.65±0.3	7.81±0.3	8.01±0.5	9.70±0.3	10.83±0.6	11.53±0.2	10.69±0.9
	EA	8.70±0.0	9.51±0.4	9.58±0.7	9.26±0.6	11.92±0.3	11.31±1.0	10.26±0.3	11.16±0.9
	Average	8.01±1.2				10.43±1.1			

TABLE VI

SUMMARY OF POWER CONSUMPTION (%) FOR TORQUE AND CADENCE CONTROL USING ASTW AND STW CONTROLLERS WITH BOTH THE FIXED AND THE PROPOSED STIMULATION PATTERNS ON THREE SPINAL CORD INJURY SUBJECTS FOR THREE DAYS

Stimulation Pattern	Subject	ASTW				STW			
		Day1	Day2	Day3	mean	Day1	Day2	Day3	mean
Proposed	AA	37.0±1.1	34.2±0.3	37.2±0.5	36.1±1.6	38.3±1.1	39.5±1.1	38.7±0.9	38.8±1.0
	HD	42.4±1.2	44.0±1.8	44.6±1.1	43.6±1.5	44.8±2.5	46.3±2.0	43.0±4.0	44.7±2.7
	EA	34.7±2.0	37.3±2.3	35.8±3.9	35.9±2.5	37.3±3.8	40.0±0.1	38.4±0.8	38.5±2.1
	Average	38.6±4.1				40.7±3.5			
Fixed	AA	47.3±1.4	52.0±1.7	49.0±0.5	49.4±2.3	55.1±2.2	53.5±1.6	53.9±4.0	54.1±2.3
	HD	51.0±2.2	53.9±1.0	52.7±3.3	52.5±2.3	57.7±2.5	55.8±1.0	60.7±0.5	58.1±2.6
	EA	53.3±2.0	46.4±2.7	47.4±2.4	49.1±3.8	53.2±3.2	55.3±3.7	58.2±4.5	55.6±3.8
	Average	50.3±3.2				55.9±3.2			

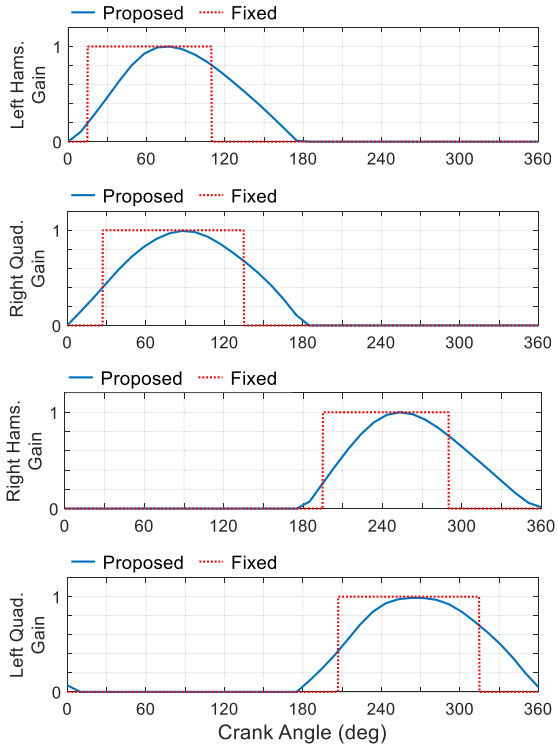

Fig. 6. Fixed and proposed stimulation patterns for the left hamstrings, right quadriceps, right hamstrings, and the left quadriceps over a crank cycle.

controller is used for control of all the muscles (Fig. 6), the gain of each muscle input is adjusted by the proposed stimulation pattern.

The average of cadence tracking errors over all subjects and all trials of the experiment are 5.77±0.5% and 7.79±0.9% using ASTW with proposed and fixed stimulation patterns, respectively, while the cadence errors are 6.21±0.5% and 8.44±1.0% using STW algorithm with proposed and fixed patterns, respectively. Table V summarizes the average of torque tracking error for three sessions on three SCI subjects using STW or ASTW controllers with both the proposed and the fixed stimulation patterns. The average of NRMS errors obtained using ASTW and STW with the proposed stimulation pattern are 5.23±0.8% and 5.94±0.9%, respectively. The ASTW controller improved the tracking performance by 12.0% compared to the STW ($p = 0.002$). Compared to the fixed stimulation pattern, the proposed stimulation pattern significantly improved the tracking performance by 34.7% using ASTW and by 43.1% using STW ($p < 0.001$).

The power consumptions of the ASTW and STW with proposed stimulation pattern are 38.6±4.1 and 40.7±3.5, respectively (Table VI). Compared to the fixed stimulation pattern, the proposed stimulation pattern significantly reduces the power consumption by 23.3% using ASTW algorithm ($p < 0.001$) and by 27.19% using the STW ($p < 0.001$). The results show that the stimulation pattern significantly affects the power consumption.

IV. DISCUSSION AND CONCLUSION

In this paper, a method was proposed for determining the stimulation pattern. In contrast to the previous study [20], the method does not require to measure anthropometric

dimensions of the subject (i.e., length of thigh and shank) and the bicycle-ride parameters (i.e., the horizontal length from hip to crank, vertical length from hip to crank, and length of the crank). The proposed method was just based on measuring the joint angles. Moreover, the method could automatically determine the gain of each muscle contributing to the cycling. The results of the simulation and experimental studies show that the proposed method provides good tracking performance and efficient power use compared to the fixed stimulation pattern. Reducing the power consumption could reduce muscle fatigue and increase cycling endurance.

An important issue of FES-cycling is the control strategy. The previous methods for the closed-loop control of FES-cycling require off-line identification before they can be used for real-time control [9], [13]. The burdens of pre-training and pre-adjustment of the controller may limit the clinical applications of these methods. Moreover, inaccurate adjustment of the parameters and estimation error could reduce the performance of the controller.

A major advantage of the proposed control framework is that it is free from mathematical modeling of the plant under study as well as from off-line learning phase. The parameters of the controller are automatically adjusted on-line. Moreover, the proposed control scheme does not require to know the boundary of the perturbations. The control gains are adapted on-line to the unknown additive and multiplicative perturbation. The results clearly indicate that perfect cadence and torque tracking performance was achieved without using any subject-specific model information.

REFERENCES

[1] P. H. Peckham, "Functional electrical stimulation: Current status and future prospects of applications to the neuromuscular system in spinal cord injury," *Paraplegia*, vol. 25, no. 3, pp. 279–288, Jun. 1987.

[2] T. A. Perkins, N. N. Donaldson, N. A. C. Hatcher, I. D. Swain, and D. E. Wood, "Control of leg-powered paraplegic cycling using stimulation of the lumbo-sacral anterior spinal nerve roots," *IEEE Trans. Neural Syst. Rehabil. Eng.*, vol. 10, no. 3, pp. 158–164, Sep. 2002.

[3] C.-W. Peng *et al.*, "Review: Clinical benefits of functional electrical stimulation cycling exercise for subjects with central neurological impairments," *J. Med. Biol. Eng.*, vol. 31, no. 1, pp. 1–11, Jan. 2011.

[4] C. Fattal *et al.*, "Training with FES-assisted cycling in a subject with spinal cord injury: Psychological, physical and physiological considerations," *J. Spinal Cord Med.*, vol. 43, no. 3, pp. 402–413, May 2018.

[5] T. Mohr, J. Pødenphant, F. Biering-Sørensen, H. Galbo, G. Thamsborg, and M. Kjær, "Increased bone mineral density after prolonged electrically induced cycle training of paralyzed limbs in spinal cord injured man," *Calcified Tissue Int.*, vol. 61, no. 1, pp. 22–25, Jul. 1997.

[6] C. Ferrario, K. J. Hunt, S. Grant, A. N. McLean, M. H. Fraser, and D. B. Allan, "Control approach for high sensitivity cardiopulmonary exercise testing during stimulated cycle ergometry in spinal cord injured subjects," *Biomed. Signal Process. Control*, vol. 2, no. 4, pp. 311–322, Oct. 2007.

[7] L. Griffin *et al.*, "Functional electrical stimulation cycling improves body composition, metabolic and neural factors in persons with spinal cord injury," *J. Electromyogr. Kinesiol.*, vol. 19, no. 4, pp. 614–622, Aug. 2009.

[8] A. Frotzler *et al.*, "High-volume FES-cycling partially reverses bone loss in people with chronic spinal cord injury," *Bone*, vol. 43, no. 1, pp. 169–176, Jul. 2008.

[9] K. J. Hunt *et al.*, "Control strategies for integration of electric motor assist and functional electrical stimulation in paraplegic cycling: Utility for exercise testing and mobile cycling," *IEEE Trans. Neural Syst. Rehabil. Eng.*, vol. 12, no. 1, pp. 89–101, Mar. 2004.

[10] M. Grohler, T. Angeli, T. Eberharter, P. Lugner, W. Mayr, and C. Hofer, "Test bed with force-measuring crank for static and dynamic investigations on cycling by means of functional electrical stimulation," *IEEE Trans. Neural Syst. Rehabil. Eng.*, vol. 9, no. 2, pp. 169–180, Jun. 2001.

[11] K. J. Hunt *et al.*, "Comparison of stimulation patterns for FES-cycling using measures of oxygen cost and stimulation cost," *Med. Eng. Phys.*, vol. 28, no. 7, pp. 710–718, Sep. 2006.

[12] L. M. Schutte, M. M. Rodgers, F. E. Zajac, and R. M. Glaser, "Improving the efficacy of electrical stimulation-induced leg cycle ergometry: An analysis based on a dynamic musculoskeletal model," *IEEE Trans. Rehabil. Eng.*, vol. 1, no. 2, pp. 109–125, Jun. 1993.

[13] N. A. Hakansson and M. L. Hull, "Muscle stimulation waveform timing patterns for upper and lower leg muscle groups to increase muscular endurance in functional electrical stimulation pedaling using a forward dynamic model," *IEEE Trans. Biomed. Eng.*, vol. 56, no. 9, pp. 2263–2270, Sep. 2009.

[14] C.-S. Kim *et al.*, "Stimulation pattern-free control of FES cycling: Simulation study," *IEEE Trans. Syst., Man, Cybern. C, Appl. Rev.*, vol. 38, no. 1, pp. 125–134, Jan. 2008.

[15] M. Gfohler and P. Lugner, "Dynamic simulation of FES-cycling: Influence of individual parameters," *IEEE Trans. Neural Syst. Rehabil. Eng.*, vol. 12, no. 4, pp. 398–405, Dec. 2004.

[16] E. S. Idsø, T. Johansen, and K. J. Hunt, "Finding the metabolically optimal stimulation pattern for FES-cycling," in *Proc. Conf. Int. Funct. Elect. Stimulation Soc.*, Bournemouth, U.K., Sep. 2004, pp. 1–3.

[17] J. J. Chen, N.-Y. Yu, D.-G. Huang, B.-T. Ann, and G.-C. Chang, "Applying fuzzy logic to control cycling movement induced by functional electrical stimulation," *IEEE Trans. Rehabil. Eng.*, vol. 5, no. 2, pp. 158–169, Jun. 1997.

[18] J.-J. E. Slotine and W. Li, *Applied Nonlinear Control*. Englewood Cliffs, NJ, USA: Prentice-Hall, 1991.

[19] Y. Shtessel, C. Edwards, L. Fridman, and A. Levant, *Sliding Mode Control and Observation*. Secaucus, NJ, USA: Birkhäuser, 2012.

[20] M. J. Bellman, T.-H. Cheng, R. J. Downey, C. J. Hass, and W. E. Dixon, "Switched control of cadence during stationary cycling induced by functional electrical stimulation," *IEEE Trans. Neural Syst. Rehabil. Eng.*, vol. 24, no. 12, pp. 1373–1383, Dec. 2016.

[21] M. J. Bellman, R. J. Downey, A. Parikh, and W. E. Dixon, "Automatic control of cycling induced by functional electrical stimulation with electric motor assistance," *IEEE Trans. Autom. Sci. Eng.*, vol. 14, no. 2, pp. 1225–1234, Apr. 2017.

[22] C. A. Cousin *et al.*, "Closed-loop cadence and instantaneous power control on a motorized functional electrical stimulation cycle," *IEEE Trans. Control Syst. Technol.*, vol. 28, no. 6, pp. 2276–2291, Nov. 2020.

[23] K. D. Young, V. I. Utkin, and U. Ozguner, "A control engineer's guide to sliding mode control," *IEEE Trans. Control Syst. Technol.*, vol. 7, no. 3, pp. 328–342, May 1999.

[24] V. H. Duenas, C. A. Cousin, C. Rouse, E. J. Fox, and W. E. Dixon, "Distributed repetitive learning control for cooperative cadence tracking in functional electrical stimulation cycling," *IEEE Trans. Cybern.*, vol. 50, no. 3, pp. 1084–1095, Mar. 2020.

[25] V. H. Duenas, C. A. Cousin, A. Parikh, P. Freeborn, E. J. Fox, and W. E. Dixon, "Motorized and functional electrical stimulation induced cycling via switched repetitive learning control," *IEEE Trans. Control Syst. Technol.*, vol. 27, no. 4, pp. 1468–1479, May 2019.

[26] V. H. Duenas, C. A. Cousin, V. Ghanbari, E. J. Fox, and W. E. Dixon, "Torque and cadence tracking in functional electrical stimulation induced cycling using passivity-based spatial repetitive learning control," *Automatica*, vol. 115, May 2020, Art. no. 108852.

[27] V. Ghanbari, V. H. Duenas, P. J. Antsaklis, and W. E. Dixon, "Passivity-based iterative learning control for cycling induced by functional electrical stimulation with electric motor assistance," *IEEE Trans. Control Syst. Technol.*, vol. 27, no. 5, pp. 2287–2294, Sep. 2019.

[28] D. A. Bristow, M. Tharayil, and A. G. Alleyne, "A survey of iterative learning control," *IEEE Control Syst. Mag.*, vol. 26, no. 3, pp. 96–114, May 2006.

[29] R. W. Longman, "Iterative learning control and repetitive control for engineering practice," *Int. J. Control*, vol. 73, no. 10, pp. 930–954, Jan. 2000.

[30] C. T. Freeman, P. Sampson, J. H. Burridge, and A.-M. Hughes, "Repetitive control of functional electrical stimulation for induced tremor suppression," *Mechatronics*, vol. 32, pp. 79–87, Dec. 2015.

[31] A. Farhoud and A. Erfanian, "Fully automatic control of paraplegic FES pedaling using higher-order sliding mode and fuzzy logic control," *IEEE Trans. Neural Syst. Rehabil. Eng.*, vol. 22, no. 3, pp. 533–542, May 2014.
[32] A. Levant, "Sliding order and sliding accuracy in sliding mode control," *Int. J. Control*, vol. 58, no. 6, pp. 1247–1263, Dec. 1993.
[33] W. Perruquetti and J. P. Barbot, *Sliding Mode Control in Engineering*. New York, NY, USA: Marcel Dekker, 2002.
[34] Y. Shtessel, M. Taleb, and F. Plestan, "A novel adaptive-gain supertwisting sliding mode controller: Methodology and application," *Automatica*, vol. 48, no. 5, pp. 759–769, May 2012.
[35] A. Levant, "Higher-order sliding modes, differentiation and output-feedback control," *Int. J. Control*, vol. 76, nos. 9–10, pp. 924–941, Jan. 2003.
[36] A. Levant, "Homogeneity approach to high-order sliding mode design," *Automatica*, vol. 41, no. 5, pp. 823–830, May 2005.
[37] L. X. Wang, *Adaptive Fuzzy Systems and Control*. Englewood Cliffs, NJ, USA: Prentice-Hall, 1994.
[38] E. S. Idsø, "Development of a mathematical model of a rider-tricycle system," Dept. Eng. Cybern., Norwegian Univ. Sci. Technol., Trondheim, Norway, Tech. Rep., 2002.
[39] M. Gföhler and P. Lugner, "Cycling by means of functional electrical stimulation," *IEEE Trans. Rehabil. Eng.*, vol. 8, no. 2, pp. 233–243, Jun. 2000.
[40] J. J. Abbas and H. J. Chizeck, "Neural network control of functional neuromuscular stimulation systems: Computer simulation studies," *IEEE Trans. Biomed. Eng.*, vol. 42, no. 11, pp. 1117–1127, Nov. 1995.
[41] A. Damiano, G. L. Gatto, I. Marongiu, and A. Pisano, "Second-order sliding-mode control of DC drives," *IEEE Trans. Ind. Electron.*, vol. 51, no. 2, pp. 364–373, Apr. 2004.
[42] S. C. Abdulla, O. Sayidmarie, and M. O. Tokhi, "Functional electrical stimulation-based cycling assisted by flywheel and electrical clutch mechanism: A feasibility simulation study," *Robot. Auto. Syst.*, vol. 62, no. 2, pp. 188–199, Feb. 2014.
[43] A. Erfanian, H.-R. Kobravi, O. Zohorian, and F. Emani, "A portable programmable transcutaneous neuroprosthesis with built-in self-test capability for training and mobility in paraplegic subjects," in *Proc. 11th Ann. Conf. Int. Funct. Elect. Stimulation Soc.*, Zao, Japan, Sep. 2006, pp. 1–3.
[44] N. Kirsch, N. Alibeji, B. E. Dicianno, and N. Sharma, "Switching control of functional electrical stimulation and motor assist for muscle fatigue compensation," in *Proc. Amer. Control Conf. (ACC)*, Jul. 2016, pp. 4865–4870.
[45] N. Kirsch, "Control methods for compensation and inhibition of muscle fatigue in neuroprosthetic devices," Ph.D. dissertation, Dept. Mech. Eng. Mater. Sci., Swanson School Eng., Univ. Pittsburgh, Pittsburgh, PA, USA, 2016.
[46] M. K. E. Khine, M. W. M. Htwe, and M. Y. Y. Mon, "Simulation DC motor speed control system by using PID controller," *Int. J. Trend Sci. Res. Develop.*, vol. 3, no. 4, pp. 1418–1423, 2019.
[47] J. Agajo, P. N. Okoro, A. O. Akande, and T. A. Folorunso, "Modelling of dynast simulator to controlling speed in a DC motor using proportional integral derivative controller," *Amer. Sci. Res. J. Eng., Technol., Sci.*, vol. 14, no. 1, pp. 64–76, Oct. 2015.
[48] D. B. McCreery, W. F. Agnew, T. G. H. Yuen, and L. Bullara, "Charge density and charge per phase as cofactors in neural injury induced by electrical stimulation," *IEEE Trans. Biomed. Eng.*, vol. 37, no. 10, pp. 996–1001, Oct. 1990.
[49] C. Günter, J. Delbeke, and M. Ortiz-Catalan, "Safety of long-term electrical peripheral nerve stimulation: Review of the state of the art," *J. Neuroeng. Rehabil.*, vol. 16, no. 1, p. 13, Dec. 2019.